GSA Data Repository 2019312

Grossman, E.L., et al., 2019, Freshwater input, upwelling, and the evolution of Caribbean coastal ecosystems during formation of the Isthmus of Panama: Geology, https://doi.org/10.1130/G46357.1

SUPPLEMENTAL MATERIALS

Freshwater input, upwelling, and the evolution of Caribbean coastal ecosystems during formation of the Isthmus of Panama

Ethan L. Grossman[1], John A. Robbins[1*], Paola G. Rachello-Dolmen[1,2], Kai Tao[1], Divya Saxena[1], and Aaron O'Dea[2]

[1] *Department of Geology and Geophysics, Texas A&M University, College Station, TX, USA 77843*

[2] *Naos Island Marine Laboratory, Smithsonian Tropical Research Institute, PO Box 0843-03092 Balboa, Panama*

[*] Corresponding author: e-grossman@tamu.edu

METHODS

Sampling Methods

A 0.5 dental drill was used to collect sample powders in holes or along shallow grooves on growth lines in ontogenetic sequence on the spire of the gastropod shells (Figure S1). Sample grooves were used for larger samples (~200 µg) necessary for trace element analyses (data not reported). Representative oxygen and carbon isotopic profiles of modern and fossil gastropod shells are shown in Figure S2.

Baseline Calculations

To reference nearshore and shelf environments to open ocean conditions, we normalized the

$\delta^{18}O$ profiles of fossil specimens for each fossil locality to the $\delta^{18}O$ values of coeval planktonic foraminifera from deep sea cores. Following the approach of Tao et al. (2013) for modern shells, gastropod $\delta^{18}O$ profiles were referenced to open ocean baselines using $\delta^{18}O$ measurements of coeval, depth-equivalent planktonic foraminifera from deep-sea cores collected from the same region. The method assumes that planktonic foraminiferal $\delta^{18}O$ represents open ocean conditions free of seasonal upwelling and freshening. Though planktonic foraminifera can show seasonal growth patterns, foraminifera from lower latitudes (±20°), and *G. ruber* (white) and *G. sacculifer* in particular, are most suitable for estimating mean annual SST (Fraile et al., 2009). Foraminiferal $\delta^{18}O$ values were equated to gastropod shell aragonite by correcting for aragonite-calcite fractionation ($\varepsilon_{cc\text{-}ar} = 0.8‰$; Grossman and Ku, 1986).

To test this method, we compared baseline $\delta^{18}O$ values for modern *Conus* localities, determined using logger and WOA data (Tao et al., 2013), with values determined from the $\delta^{18}O$ of foraminifera from sediment core-tops. The baselines generated using the two techniques fall along the 1:1 line (Table S2, Figure S3).

Foraminiferal $\delta^{18}O$ values for the Plio-Pleistocene were obtained from sediment cores ODP 999A (Haug et al., 2001; Steph et al., 2010), DSDP 502B (Prell, 1982), and MD03-2628 (Sepulcre et al., 2011) in the Caribbean and ODP 1241 (Steph et al., 2006), ODP 111-677A,B (Shackleton and Hall, 1989), and ODP 851 (Cannariato and Ravelo, 1997; Ravelo and Shackleton, 1995) in the Pacific (Figure 1). For specimens from depths of 30 m or less, *G. ruber* (white) isotope values were used as the baseline. Specimens with median depths of 50-60 m were normalized using data from *G. sacculifer* foraminifera. For specimens from waters between 100 and 150 m deep, *N. dutertrei* was used. Specimens from 50-100 m deep were normalized using an average of *G. sacculifer* and *N. dutertrei* values. Baselines for shallow water (<30 m) specimens from La Bomba, Río Limoncito, and Wild Cane Key were determined by adding the average difference between *G. ruber* (white) and *G. sacculifer* foraminifera measurements from 0.5 to 1.0 Ma (-0.16‰; data from Prell, 1982; Sepulcre et al., 2011) to the average of all *G. sacculifer* measurements from ODP 999 over the interval of time represented by the locality. The interval from 0.5 to 1.0 Ma was used because it predates the most severe fluctuations in marine $\delta^{18}O$ associated with glaciation (Lisiecki and Raymo, 2005) and goes back as far as the *G. ruber* isotope record exists in this region. No *G. sacculifer* measurements are available for the interval in which Wild Cane Key was deposited, so an average of *G. sacculifer* measurements from 500 kyr before and after was used. Specimens from Isla Popa and La Peña used the average $\delta^{18}O$ of *G. sacculifer* specimens from their respective cores and intervals of time (Haug et al., 2001; Steph et al., 2006). All values were converted from calcite to aragonite by adding 0.8‰ (Grossman and Ku, 1986).

We averaged the means of *G. sacculifer* and *N. dutertrei* data from the appropriate intervals to calculate baselines for localities that fall between 50-100 m paleodepth. These localities include Lower Lomas del Mar, Fish Hole, Isla Solarte, Punta Norte East, and Punta Tiburon to Punta Piedra. For younger localities (Upper Lomas del Mar and Pueblo Nuevo Cemetery), *N. dutertrei* data were not available for the entire interval of interest. For Upper Lomas del Mar (1.5-1.7 Ma), the averages of *G. sacculifer* and *N. dutertrei* data from 2.5 to 3.0 Ma (Haug et al., 2001; Steph et al., 2010) were averaged to determine the offset between that average (-0.65‰) and the *G. sacculifer* average (-0.91‰), which was -0.26‰. This value was then subtracted from the average of *G. sacculifer* $\delta^{18}O$ measurements from 1.5-1.7 Ma (Prell, 1982) to determine the baseline for Upper Lomas del Mar. The same offset was used to calculate the baseline for Pueblo Nuevo Cemetery, but was subtracted from the average of *G. sacculifer* $\delta^{18}O$ measurements from

1.3-1.8 Ma (Prell, 1982) and 2.2-2.7 Ma (Haug et al., 2001). We used the average of *N. dutertrei* $\delta^{18}O$ measurements (Steph et al., 2010) over the interval of interest (3.5 to 5.0 Ma) to calculate baselines for deep water localities (100-150 m; SE and NE Escudo de Veraguas).

Baseline $\delta^{18}O$ values were compared with measured $\delta^{18}O$ values (Figure S4) to produce the $\delta^{18}O_{median}$-$\delta^{18}O_{baseline}$ ($\Delta^{18}O_{med\text{-}bl}$) box-and-whisker plots (Fig. 3). Median values were used rather than averages to minimize the influence of extreme values. Error bars for each of the baseline calculations ($\varepsilon[\delta^{18}OBL]$) were determined by squaring and then summing the standard deviations (1σ) of each set of foraminiferal data ($\varepsilon[\delta^{18}OForam1\text{-}X]$) used in the calculation. The square of our own isotope analysis precision ($\varepsilon[\delta^{18}OAR]$) was added to this sum before taking the square root of the final sum. This square root represented the error in our baseline calculations.

$$\varepsilon(\delta^{18}O_{BL}) = [\varepsilon(\delta^{18}O_{AR})^2 + \varepsilon(\delta^{18}O_{Foram1})^2 + \varepsilon(\delta^{18}O_{Foram2})^2 + \ldots + \varepsilon(\delta^{18}O_{ForamX})^2]^{1/2}$$

RESULTS

All isotopic results are shown in Table S3.

Carbon Isotopes and $\delta^{18}O$-$\delta^{13}C$ Correlations

Carbon isotope profiles in these Plio-Pleistocene specimens have proved difficult to interpret and merit additional study. Median values ranged from -1.3 to 2.7‰ except for three *Conus* specimens from Punta Nispero (H19694, H19707, H19715), which yielded median values of -5.8, -6.0, and -16.0‰ (Fig. S5). These ^{13}C-depleted specimens remain enigmatic, and may reflect oxidation of buried plant matter, including logs, found at Punta Nispero (Collins ant Coates, 1999). Unfortunately, we do not have detailed sedimentological data collected with these shells. Excluding the shells, the second most important factor controlling $\delta^{13}C$ is taxonomy, with *Strombus* shells mostly <0‰ and *Conus* mostly >0‰. Carbon isotope composition does not correlate with age or paleodepth.

Previous studies have used $\delta^{18}O$-$\delta^{13}C$ correlations (R_{O-C}) and $\delta^{18}O$ range as proxies for freshening and upwelling, with mixed results (e.g., Killingley and Berger, 1979; Jones and Allmon, 1995; Tao et al., 2013; Anderson et al., 2017). We see no significant correlation between R_{O-C} and $\delta^{18}O$ range, or between R_{O-C} and $\Delta^{18}O_{med-bl}$ for the entire data set and for individual sample localities, age groups, or paleo-depths (Figures S6, S7). In localities influenced by seasonal freshening and upwelling, the freshwater signal can swamp the upwelling signal, resulting in a positive O-C correlation (Tao et al., 2013). However, in special cases like beach-collected shells from the modern Pacific, the isotopic record can be parsed by $\delta^{18}O$ into two segments, with positive correlation in the low $\delta^{18}O$ segment (rainy season) and negative correlation in the high $\delta^{18}O$ segment (dry, upwelling season; Graniero et al., 2017). Such trends, however, can be lost in shells from greater water depth where $\delta^{18}O$ range is reduced and other influences like vital effects (physiological processes) and flux of microbial CO_2 from organic-rich sediments complicate the carbon isotope record.

PALEOLATITUDE

To ensure that changes in rainfall patterns can be safely ascribed to shifts in the ITCZ rather than plate movements, we determined paleolatitudes for the study area. Paleolatitude has changed little (<0.2° latitude) in the last 6 Ma (GPlates, 2017, https://www.gplates.org/; PALEOMAP PaleoAtlas for GPlates, 2016, ftp://ftp.earthbyte.org/earthbyte/PaleoAtlas_Scotese_v2.zip).

REFERENCES

Anderson, B. M., Hendy, A., Johnson, E. H., and Allmon, W. D., 2017, Paleoecology and paleoenvironmental implications of turritelline gastropod-dominated assemblages from the Gatun Formation (Upper Miocene) of Panama: Palaeogeography, Palaeoclimatology, Palaeoecology, v. 470, p. 132-146.

Benway, H. M., Mix, A. C., Haley, B. A., and Klinkhammer, G. P., 2006, Eastern Pacific Warm Pool paleosalinity and climate variability: 0-30 kyr: Paleoceanography, v. 21, no. 3.

Cannariato, K. G., and Ravelo, A. C., 1997, Pliocene-Pleistocene evolution of eastern tropical Pacific surface water circulation and thermocline depth: Paleoceanography, v. 12, no. 6, p. 805-820.

Collins, L.S., and Coates, A.G., 1999, A paleobiotic survey of Caribbean faunas from the Neogene of the Isthmus of Panama. Bulletin of American Paleontology, no. 357, Ithaca, 351 pp.

Conkright, M. E., Locarnini, R. A., Garcia, H. E., O'Brien, T. D., Boyer, T. P., Stephens, C., and Antonov, J. I., 2002, World Ocean Atlas 2001: Objective analyses, data statistics, and figures, *in* Center, N. O. D., ed.: Silver Spring, MD, National Oceanographic Data Center.

Durazzi, J. T., 1981, Stable-isotope studies of planktonic-foraminifera in North-Atlantic core tops: Palaeogeography Palaeoclimatology Palaeoecology, v. 33, no. 1-3, p. 157-172.

Fraile, I., Mulitza, S., and Schulz, M., 2009, Modeling planktonic foraminiferal seasonality: Implications for sea-surface temperature reconstructions: Marine Micropaleontology, v. 72, no. 1, p. 1-9.

GPlates, 2017, https://www.gplates.org/ (April 2017).

Graniero, L.E., Grossman, E.L., Robbins, J.A., Morales, J., Thompson, R., and O'Dea, A., 2017, *Conus* shell $\delta^{13}C$ values as proxies for $\delta^{13}C_{DIC}$ in tropical waters. Palaeogeography

Palaeoclimatology Palaeoecology, v. 472, p. 119-127.

Grossman, E. L., and Ku, T. L., 1986, Oxygen and carbon isotope fractionation in biogenic aragonite – Temperature effects: Chemical Geology, v. 59, no. 1, p. 59-74.

Haug, G. H., Tiedemann, R., Zahn, R., and Ravelo, A. C., 2001, Role of Panama uplift on oceanic freshwater balance: Geology, v. 29, no. 3, p. 207-210.

Killingley, J. S., and Berger, W. H., 1979, Stable isotopes in a mollusk shell - Detection of upwelling events: Science, v. 205, no. 4402, p. 186-188.

Jones, D. S., and Allmon, W. D., 1995, Records of upwelling, seasonality and growth in stable-isotope profiles of Pliocene mollusk shells from Florida: Lethaia, v. 28, no. 1, p. 61-74.

Lisiecki, L. E., and Raymo, M. E., 2005, A Pliocene-Pleistocene stack of 57 globally distributed benthic $\delta^{18}O$ records: Paleoceanography, v. 20, no. 1.

PALEOMAP PaleoAtlas for GPlates, 2016, ftp://ftp.earthbyte.org/earthbyte/PaleoAtlas_Scotese_v2.zip (April 2017)

Prell, W. L., 1982, Oxygen and carbon isotope stratigraphy for the Quaternary of Hole 502B: evidence for two modes of isotopic variability: Init. Rep. DSDP, v. 68, p. 455-464.

Ravelo, A., and Shackleton, N., 1995, Evidence for surface-water circulation changes at Site 851 in the east equatorial Pacific, in Proceedings Proceeding of the Ocean Drilling Program, Scientific Results, v. 138, p. 503-514.

Schmidt, M. W., Spero, H. J., and Lea, D. W., 2004, Links between salinity variation in the Caribbean and North Atlantic thermohaline circulation: Nature, v. 428, no. 6979, p. 160-163.

Sepulcre, S., Vidal, L., Tachikawa, K., Rostek, F., and Bard, E., 2011, Sea-surface salinity variations in the northern Caribbean Sea across the Mid-Pleistocene Transition: Climate of the Past, v. 7, no. 1, p. 75-90.

Shackleton, N., and Hall, M., 1989, Stable isotope history of the Pleistocene at ODP Site 677, in Proceedings of the Ocean Drilling Program: Scientific results , v. 111, p. 295-316.

Steph, S., Tiedemann, R., Groeneveld, J., Sturm, A., and Nürnberg, D., 2006, Pliocene changes in tropical east Pacific upper ocean stratification: Response to tropical gateways?: Proc. ODP, Sci. Results, v. 202, p. 1-51.

Steph, S., Tiedemann, R., Prange, M., Groeneveld, J., Schulz, M., Timmermann, A., Nurnberg, D., Ruhlemann, C., Saukel, C., and Haug, G. H., 2010, Early Pliocene increase in thermohaline overturning: A precondition for the development of the modern equatorial Pacific cold tongue: Paleoceanography, v. 25, no. 2.

Tao, K., Robbins, J. A., Grossman, E. L., and O'Dea, A., 2013, Quantifying upwelling and freshening in nearshore tropical environments using stable isotopes in modern Tropical American mollusks: Bulletin of Marine Science, v. 89, p. 815-835.

SUPPLEMENTAL FIGURE CAPTIONS

Figure S1. Photographs of representative *Conus* shells viewed from above (spire) and from the side with aperture. Specimens were sampled using a 0.5-mm dental bur in a series of grooves parallel to growth bands (AT06-5-1A) or in a series of narrow-diameter holes (H19711).

Figure S2. Representative oxygen and carbon isotopic profiles of modern and fossil gastropod shells. Lengths are spiral distance from the protoconch to the lip (growth direction). The spire top was not sampled in most specimens because the shell was too thin to avoid penetration of the inner shell layer. Modern shell data are from Tao et al. (2013).

Figure S3. Baseline $\delta^{18}O_{ar}$ values for each modern *Conus* specimen calculated using non-upwelling, non-freshening water conditions based on World Ocean Atlas data (x-axis; Conkright et al., 2002; Tao et al., 2013) and open-ocean core-top foraminifera $\delta^{18}O$ (y-axis). There is an excellent correlation between the baseline calculated using World Ocean Atlas data and open-ocean core-top foraminiferal $\delta^{18}O$ ($r = 0.98$, $n = 13$, $p < 10^{-8}$) $p < 0.0001$. An independent-samples t-test was conducted to compare the two variables, and there is not a significant difference ($t(24) = -0.12$, $r = 0.900$).

Figure S4. Box-and-whisker plot of $\delta^{18}O$ measurements for mollusks in this study. The box represents the median and 1st and 3rd quartiles (with mean shown as "+"), and are shaded to represent paleodepths. The circles represent the remaining data in each shell, colored based on locality (orange = Caribbean, blue = Pacific).

Figure S5. Box-and-whisker plot of $\delta^{13}C$ measurements for mollusks in this study. The box represents the median and 1st and 3rd quartiles (with mean shown as "+"), and are shaded to represent paleodepths. The circles represent the remaining data in each shell, colored based on locality (orange = Caribbean, blue = Pacific).

Figure S6. Correlation coefficient for $\delta^{18}O$ versus $\delta^{13}C$, plotted against $\delta^{18}O$ range for 4.25-2.5 Ma and 2.5-0.1 Ma age groups and different depth categories (A: without labels, B: with labels).

Figure S7. Correlation coefficient for $\delta^{18}O$ versus $\delta^{13}C$, plotted against $\delta^{18}O$ difference between median and baseline values ($\Delta^{18}O_{Med\text{-}bl}$) for 4.25-2.5 Ma and 2.5-0.1 Ma age groups and different depth categories (A: without labels, B: with labels).

SUPPLEMENTAL TABLES

Table S1 (see separate spreadsheet). Locality, taxonomy, median age and paleodepth for each shell in this study. Baseline values and calculated errors are given, as well as references for the foraminiferal data used to calculate them (1: Steph et al., 2010; 2: Haug et al., 2001; 3: Sepulcre et al., 2011; 4: Prell, 1982; 5: Steph et al., 2006). Median values for $\delta^{18}O$ and $\delta^{13}C$, ranges for $\delta^{18}O$, C-O Pearson correlations and p-values (two-tailed test) are listed. See Table S1-v2.1.xlsx

Table S2 (below). Sample locations, depths, and baseline calculations for modern *Conus* specimens from Panamanian coastal waters using data from both the World Ocean Atlas 2001 (Conkright et al., 2002; Tao et al., 2013) and core-top foraminifera (Benway et al., 2006; Cannariato and Ravelo, 1997; Durazzi, 1981; Schmidt et al., 2004). Foraminiferal species used to calculate each baseline are listed (*Globigerinoides ruber* (white), *G. sacculifer*, and *Orbulina universa*). * Isotope measurements from sediment cores RC13-158, RC13-154, RC10-49, V26-124 were used for these calculations (Durazzi, 1981).

Shell ID	Location	Depth	WOA-derived baseline (‰)	Foram-derived baseline (‰)	Error	Foram. species	Core	Source
Southwest Caribbean								
TA06-294A	Gulf of Mosquitos	40.7	-0.66	-0.66	0.25	1	Multiple*	D
TA06-294B	Gulf of Mosquitos	40.7	-0.66	-0.66	0.25	1	"	D
SB95-1	San Blas	11	-1.26	-1.04	0.14			
TA04-10A	Bocas del Toro	15.9	-1.14	-1.04	0.14	1	"	D
TA04-10B	Bocas del Toro	15.9	-1.14	-1.04	0.14	1	"	D
TA04-10C	Bocas del Toro	15.9	-1.14	-1.04	0.14	1	"	D
Tropical Eastern Pacific								
GP97-17A	Gulf of Panama	17	-2.08	-1.78	0.22	2	ODP 1242	B
GP97-17B	Gulf of Panama	17	-2.08	-1.78	0.22	2	"	B
310474	Gulf of Panama	14.8	-1.68	-1.78	0.22	2	"	B
301490A	Gulf of Panama	10	-1.79	-1.78	0.22	2	"	B
301490B	Gulf of Panama	10	-1.79	-1.78	0.22	2	"	"
GC97-80A	Gulf of Chiriquí	61	0.20	-0.09	0.35	3	ODP 851	CR
GC97-80B	Gulf of Chiriquí	61	0.20	-0.09	0.35	3	"	CR

Species: 1 - *G. sacculifer, O. universa;* 2 - *G. ruber (white);* 3 - *G. sacculifer*

Source: D - Durazzi, 1981; B - Benway et al., 2006; CR = Cannariato and Ravelo, 1997

Table S3 (see separate spreadsheet). Compilation of all isotopic data for fossil gastropods analyzed in this study. Sample information also appears in Table S1.

Figure S1

AT06-5-1A
La Peña Fmn,
Burica Peninsula, Pacific
(~3.5 Ma)

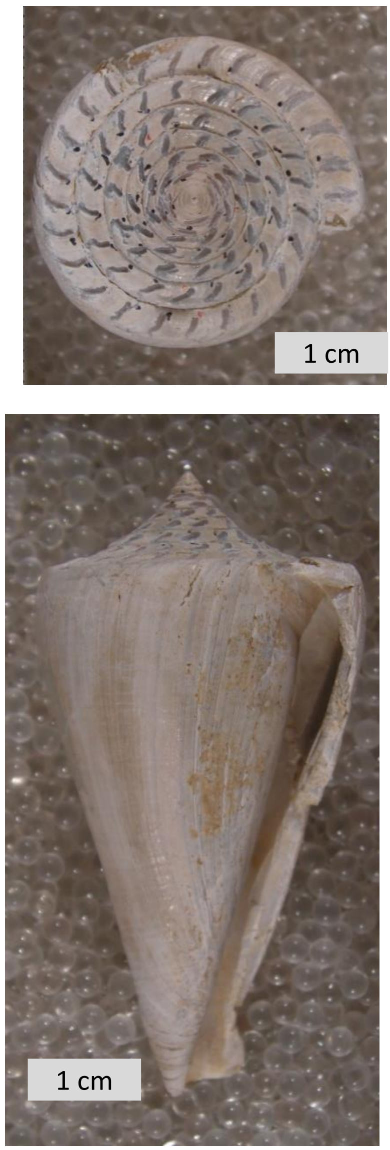

H19711
Swan Cay Fmn,
Bocas del Toro, Caribbean
(1.6-1.2 Ma)

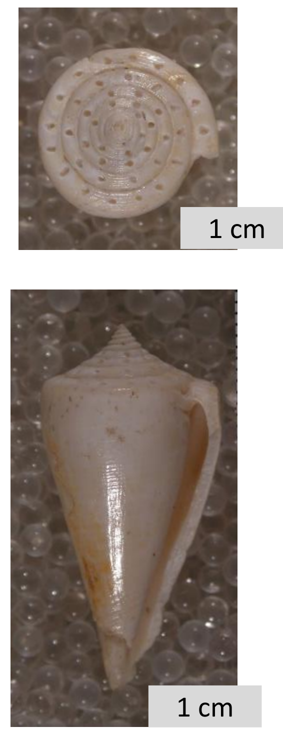

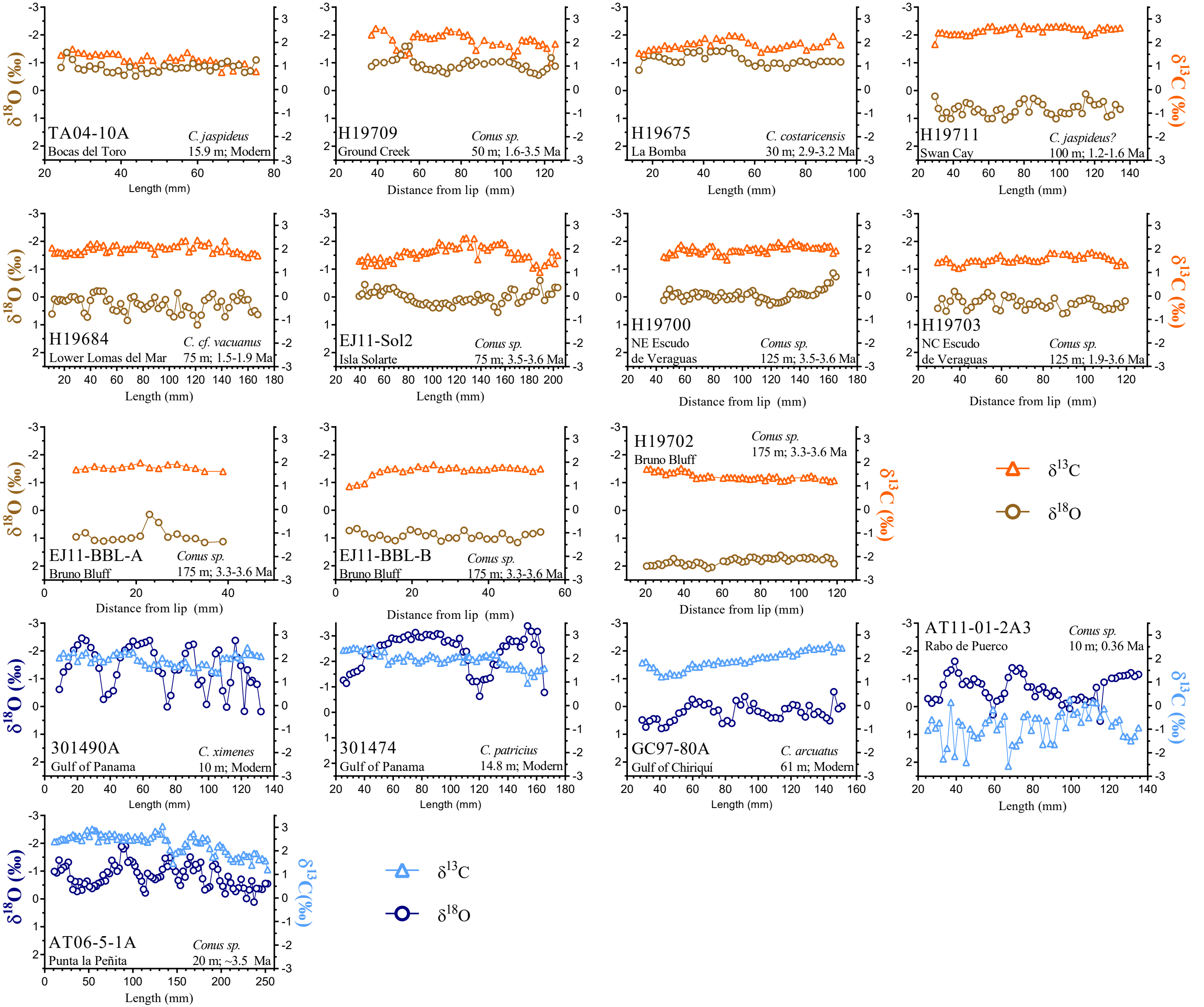

TA04-10A
C. jaspideus
Bocas del Toro
15.9 m; Modern
Length (mm)
H19709
Conus sp.
Ground Creek
50 m; 1.6-3.5 Ma
Distance from lip (mm)
H19675
C. costaricensis
La Bomba
30 m; 2.9-3.2 Ma
Length (mm)
H19711
C. jaspideus?
Swan Cay
100 m; 1.2-1.6 Ma
Length (mm)
H19684
C. cf. vacuanus
Lower Lomas del Mar
75 m; 1.5-1.9 Ma
Length (mm)
EJ11-Sol2
Conus sp.
Isla Solarte
75 m; 3.5-3.6 Ma
Length (mm)
H19700
NE Escudo de Veraguas
Conus sp.
125 m; 3.5-3.6 Ma
Distance from lip (mm)
H19703
NC Escudo de Veraguas
Conus sp.
125 m; 1.9-3.6 Ma
Distance from lip (mm)
EJ11-BBL-A
Conus sp.
Bruno Bluff
175 m; 3.3-3.6 Ma
Distance from lip (mm)
EJ11-BBL-B
Conus sp.
Bruno Bluff
175 m; 3.3-3.6 Ma
Distance from lip (mm)
H19702
Conus sp.
Bruno Bluff
175 m; 3.3-3.6 Ma
Distance from lip (mm)
δ13C
δ18O
301490A
C. ximenes
Gulf of Panama
10 m; Modern
Length (mm)
301474
C. patricius
Gulf of Panama
14.8 m; Modern
Length (mm)
GC97-80A
C. arcuatus
Gulf of Chiriquí
61 m; Modern
Length (mm)
AT11-01-2A3
Conus sp.
Rabo de Puerco
10 m; 0.36 Ma
Length (mm)
AT06-5-1A
Conus sp.
Punta la Peñita
20 m; ~3.5 Ma
Length (mm)
δ13C
δ18O
δ18O (‰)
δ13C (‰)

Figure S3

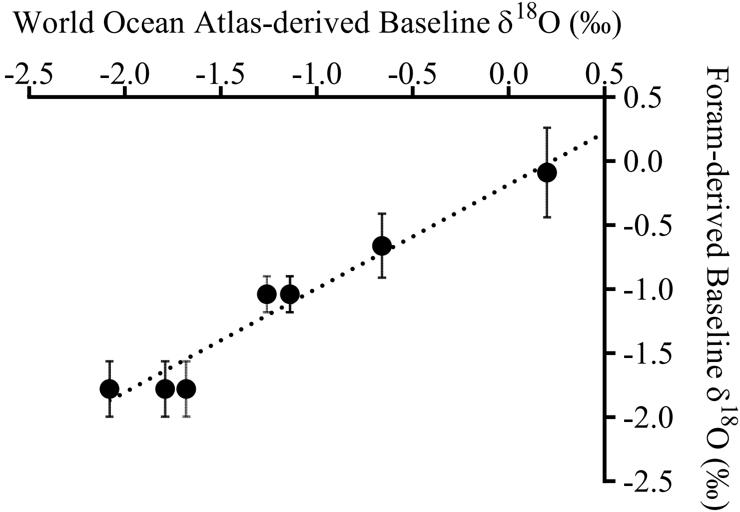

World Ocean Atlas-derived Baseline δ18O (‰)
-2.5
-2.0
-1.5
-1.0
-0.5
0.0
0.5
0.5
0.0
-0.5
-1.0
-1.5
-2.0
-2.5
Foram-derived Baseline δ18O (‰)

Figure S4

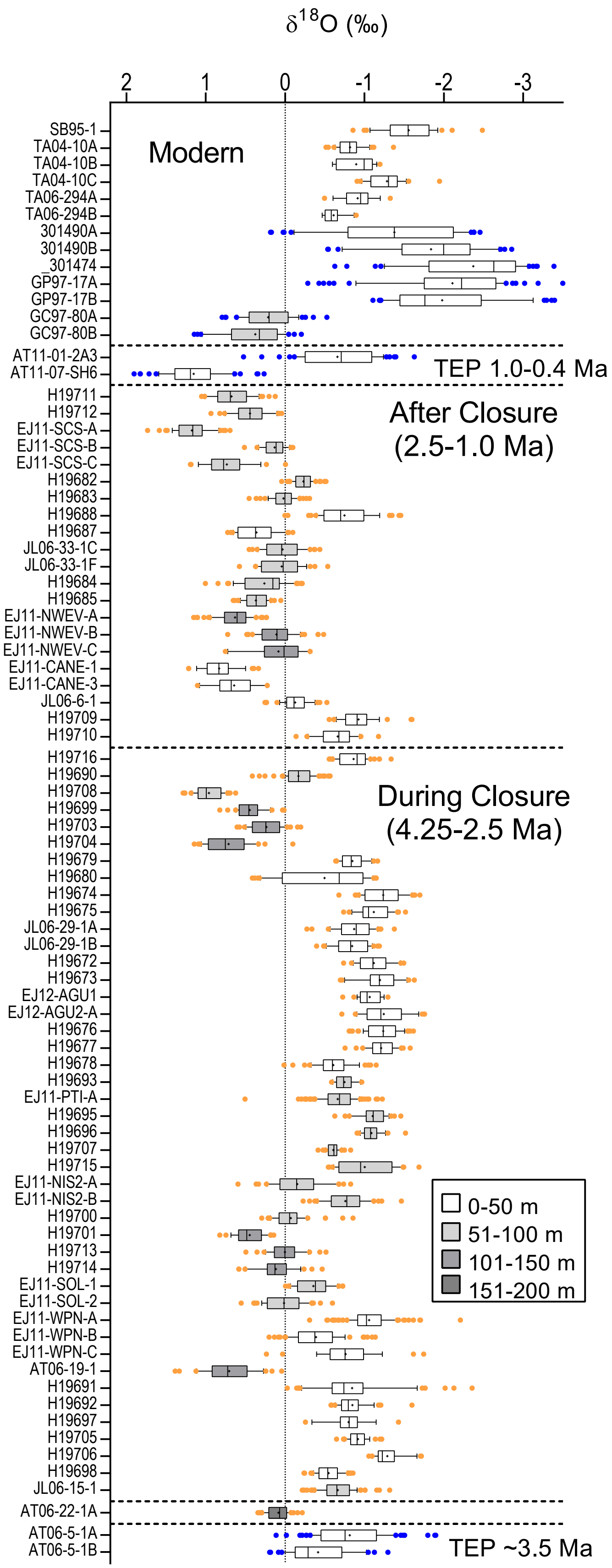

δ18O (‰)
2
1
0
-1
-2
-3
Modern
SB95-1
TA04-10A
TA04-10B
TA04-10C
TA06-294A
TA06-294B
301490A
301490B
_301474
GP97-17A
GP97-17B
GC97-80A
GC97-80B
AT11-01-2A3
AT11-07-SH6
TEP 1.0-0.4 Ma
After Closure
(2.5-1.0 Ma)
H19711
H19712
EJ11-SCS-A
EJ11-SCS-B
EJ11-SCS-C
H19682
H19683
H19688
H19687
JL06-33-1C
JL06-33-1F
H19684
H19685
EJ11-NWEV-A
EJ11-NWEV-B
EJ11-NWEV-C
EJ11-CANE-1
EJ11-CANE-3
JL06-6-1
H19709
H19710
During Closure
(4.25-2.5 Ma)
H19716
H19690
H19708
H19699
H19703
H19704
H19679
H19680
H19674
H19675
JL06-29-1A
JL06-29-1B
H19672
H19673
EJ12-AGU1
EJ12-AGU2-A
H19676
H19677
H19678
H19693
EJ11-PTI-A
H19695
H19696
H19707
H19715
EJ11-NIS2-A
EJ11-NIS2-B
H19700
H19701
H19713
H19714
EJ11-SOL-1
EJ11-SOL-2
EJ11-WPN-A
EJ11-WPN-B
EJ11-WPN-C
AT06-19-1
H19691
H19692
H19697
H19705
H19706
H19698
JL06-15-1
AT06-22-1A
AT06-5-1A
AT06-5-1B
TEP ~3.5 Ma
0-50 m
51-100 m
101-150 m
151-200 m

Figure S5

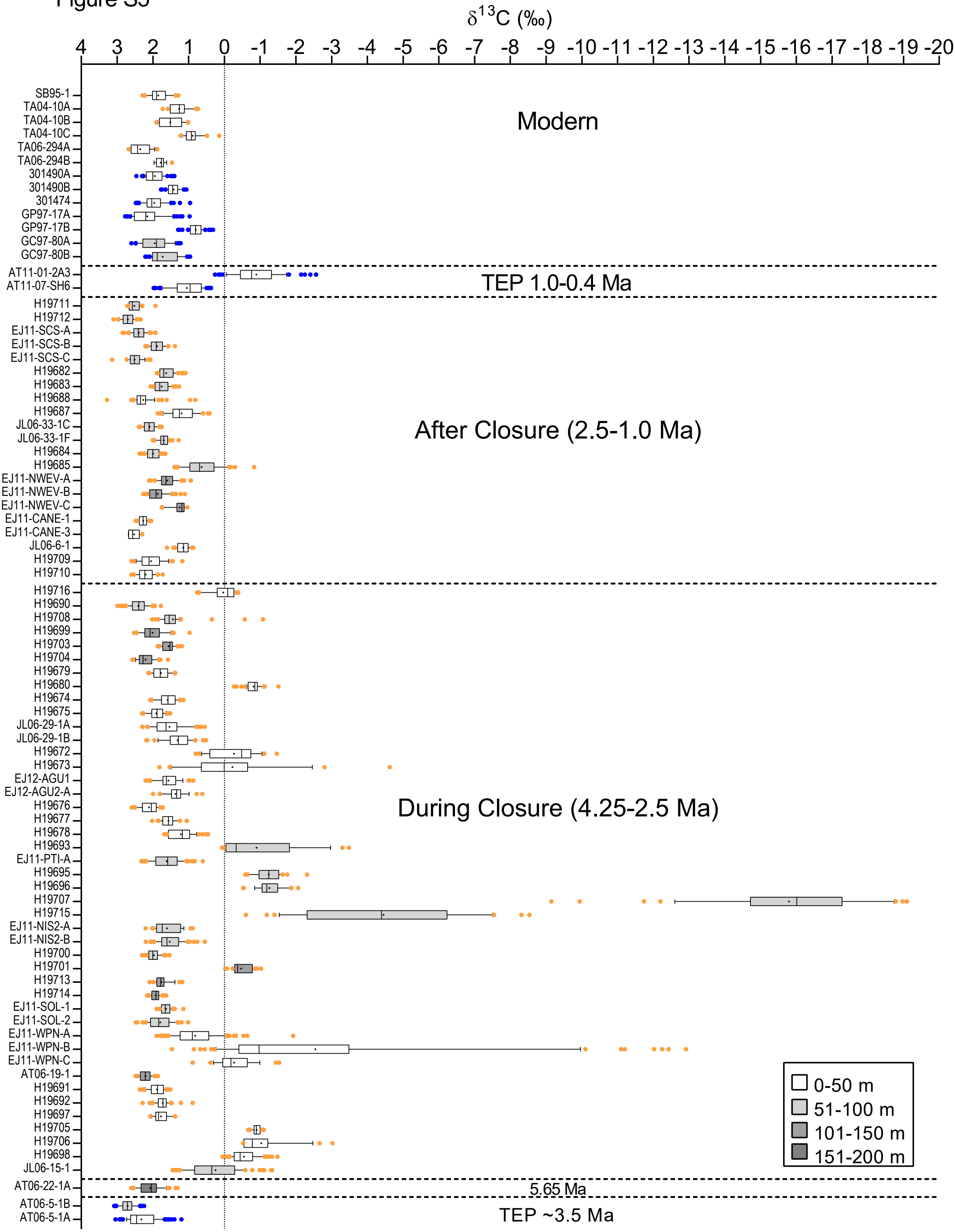

δ13C (‰)
4 3 2 1 0 -1 -2 -3 -4 -5 -6 -7 -8 -9 -10 -11 -12 -13 -14 -15 -16 -17 -18 -19 -20
Modern
SB95-1
TA04-10A
TA04-10B
TA04-10C
TA06-294A
TA06-294B
301490A
301490B
301474
GP97-17A
GP97-17B
GC97-80A
GC97-80B
TEP 1.0-0.4 Ma
AT11-01-2A3
AT11-07-SH6
After Closure (2.5-1.0 Ma)
H19711
H19712
EJ11-SCS-A
EJ11-SCS-B
EJ11-SCS-C
H19682
H19683
H19688
H19687
JL06-33-1C
JL06-33-1F
H19684
H19685
EJ11-NWEV-A
EJ11-NWEV-B
EJ11-NWEV-C
EJ11-CANE-1
EJ11-CANE-3
JL06-6-1
H19709
H19710
During Closure (4.25-2.5 Ma)
H19716
H19690
H19708
H19699
H19703
H19704
H19679
H19680
H19674
H19675
JL06-29-1A
JL06-29-1B
H19672
H19673
EJ12-AGU1
EJ12-AGU2-A
H19676
H19677
H19678
H19693
EJ11-PTI-A
H19695
H19696
H19707
H19715
EJ11-NIS2-A
EJ11-NIS2-B
H19700
H19701
H19713
H19714
EJ11-SOL-1
EJ11-SOL-2
EJ11-WPN-A
EJ11-WPN-B
EJ11-WPN-C
AT06-19-1
H19691
H19692
H19697
H19705
H19706
H19698
JL06-15-1
5.65 Ma
AT06-22-1A
TEP ~3.5 Ma
AT06-5-1B
AT06-5-1A
0-50 m
51-100 m
101-150 m
151-200 m

Figure S6

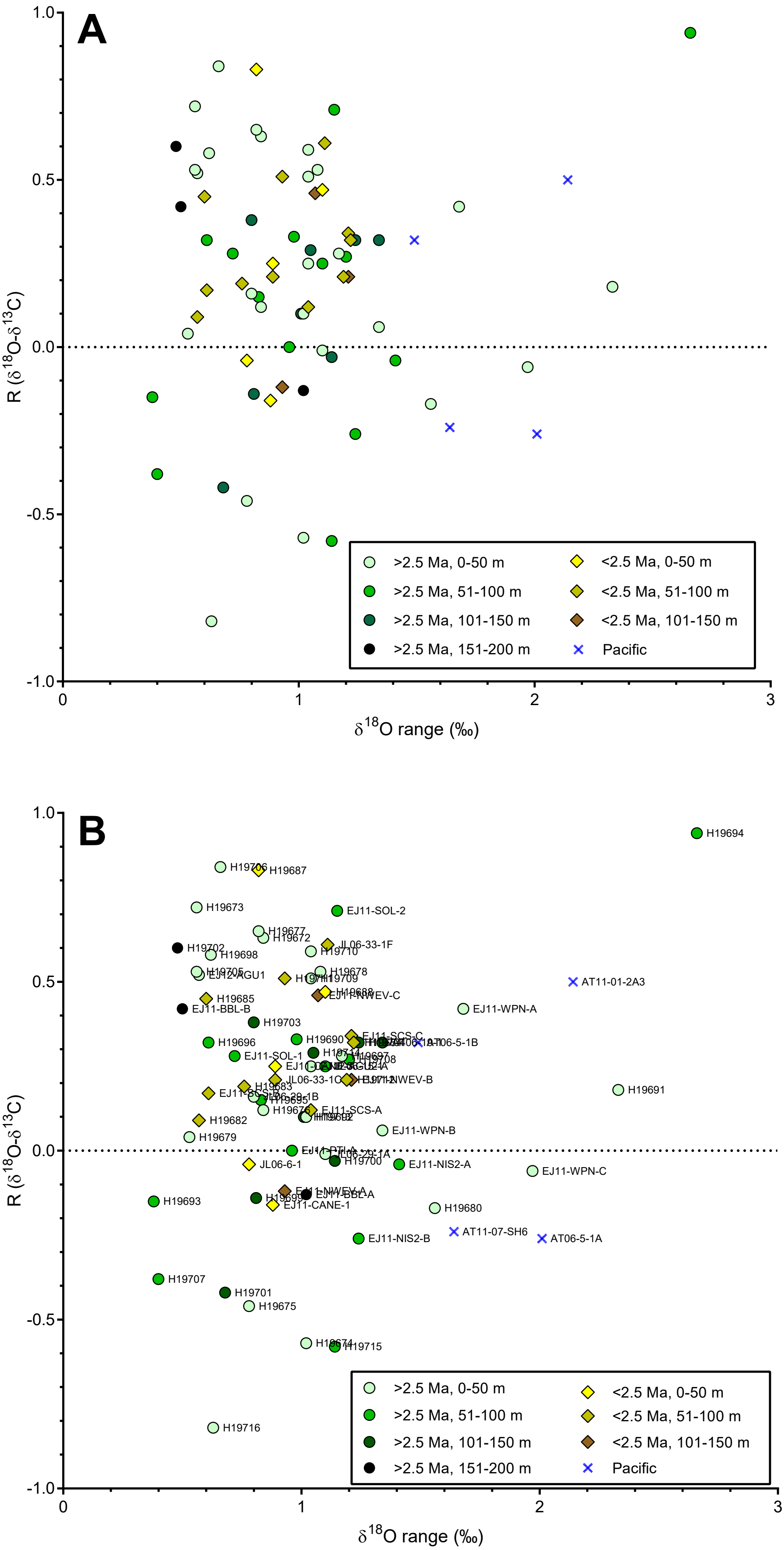
A
B
R (δ18O-δ13C)
δ18O range (‰)
1.0
0.5
0.0
-0.5
-1.0
0
1
2
3
>2.5 Ma, 0-50 m
>2.5 Ma, 51-100 m
>2.5 Ma, 101-150 m
>2.5 Ma, 151-200 m
<2.5 Ma, 0-50 m
<2.5 Ma, 51-100 m
<2.5 Ma, 101-150 m
Pacific
H19694
H19687
H19673
EJ11-SOL-2
JL06-33-1F
AT11-01-2A3
EJ11-WPN-A
H19703
H19696
EJ11-SOL-1
H19691
H19682
H19679
EJ11-WPN-B
JL06-6-1
EJ11-NIS2-A
EJ11-WPN-C
H19693
EJ11-CANE-1
H19680
AT11-07-SH6
AT06-5-1A
EJ11-NIS2-B
H19707
H19701
H19675
H19715
H19716
H19685
EJ11-BBL-B
H19698
H19700
H19690
EJ11-SCS-A

Figure S7

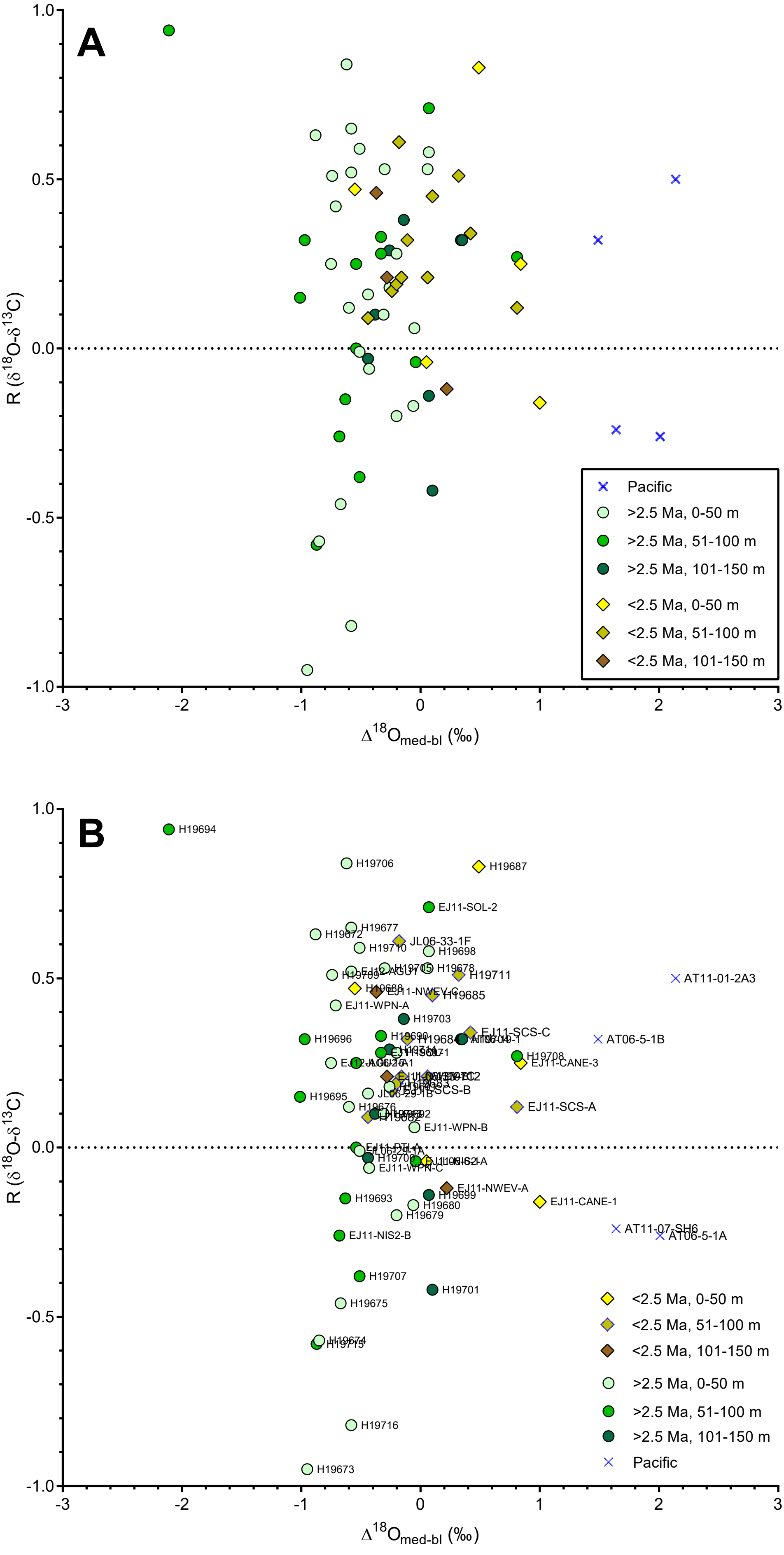
A
B
R (δ18O-δ13C)
Δ18Omed-bl (‰)
1.0
0.5
0.0
-0.5
-1.0
-3
-2
-1
0
1
2
3
Pacific
>2.5 Ma, 0-50 m
>2.5 Ma, 51-100 m
>2.5 Ma, 101-150 m
<2.5 Ma, 0-50 m
<2.5 Ma, 51-100 m
<2.5 Ma, 101-150 m
H19694
H19706
H19687
EJ11-SOL-2
H19677
H19672
JL06-33-1F
H19710
H19698
H19711
AT11-01-2A3
H19685
EJ11-WPN-A
H19703
EJ11-SCS-C
AT06-5-1B
H19696
H19708
EJ11-CANE-3
H19695
EJ11-SCS-A
EJ11-WPN-B
EJ11-WPN-C
EJ11-NWEV-A
H19699
H19680
EJ11-CANE-1
H19679
AT11-07-SH6
AT06-5-1A
H19693
EJ11-NIS2-B
H19707
H19701
H19675
H19674
H19715
H19716
H19673